

THE EFFECT OF MICRO-CHANNELS IN THE MPL ON THE PREDICTED MEMBRANE WATER CONTENT IN A PEMFC – A MODELING STUDY

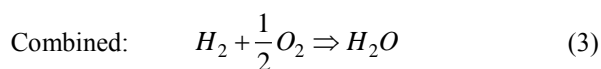
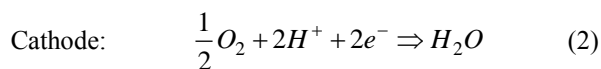
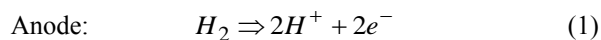
Berning, T.
 Department of Energy Technology,
 Aalborg University,
 9220 Aalborg,
 Denmark,
 E-mail: tbe@et.aau.dk

ABSTRACT

The micro-porous layer (MPL) in a proton exchange membrane fuel cell is frequently believed to constitute a barrier for the liquid water owing to its low hydraulic permeability compared to the porous substrate. When micro-channels are carved into the MPL on the side facing the catalyst layer, liquid water may be diverted from wet regions of the fuel cell to the drier inlet and outlet sections where it can evaporate and assist in hydrating the membrane as well as provide a pressure relieve at the interface between the catalyst layer and the MPL where delamination can occur under freezing conditions. This modeling study investigates the effect of such micro-channels on the predicted membrane hydration level for a predetermined set of operating conditions with a three-dimensional computational fluid dynamics model that utilizes the multi-fluid approach.

INTRODUCTION

Proton-exchange membrane fuel cells (PEMFC's) are currently being considered as an electricity source for a number of applications ranging from automotive to stationary, and their modular design allow for power ranges from several hundred kW to a few watts. These fuel cells combine internally hydrogen with oxygen from air to produce electricity, the only by-product being water and waste heat. The detailed reactions are:



These half-cell reactions occur inside the catalyst layers (CL's) on the platinum surface. The protons created in the anode side reaction migrate through a proton conducting membrane in

the center of the cell, and the electrons pass through an external electrical circle and provide electrical work. The driving potential is the cell potential. Water is created at the cathode, but when both reactant gases enter the cell dry a certain fraction of it crosses through the membrane towards the anode and humidifies the anode gas and the membrane which loses its proton conductivity when it becomes dehydrated. Figure 1 shows schematically the architecture of a PEMFC.

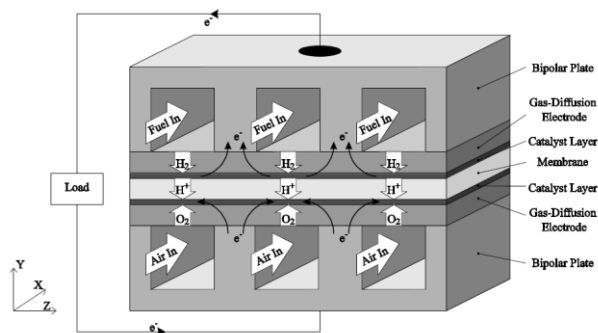


Figure 1 Schematic of a PEMFC [1].

Water management is still a problem for the successful commercialization of PEMFC's. While it is important to keep the polymer electrolyte membrane hydrated in order to ensure proton conductivity, an excess of liquid water in the cell can lead to pore plugging and prevent the reactants from reaching the catalyst layers. Just as important is to keep the outlets of the individual cells from plugging as this will lead to cell starvation in a stack. In recent work it has been found that a PEMFC may be operated in such a way that both outlet gas streams are fully humidified while entering the cell completely dry for a predetermined set of operating conditions and when the fuel cell operates at a certain target value of the water balance [2]. Such operating conditions can be found by employing dew point diagrams that show the theoretical dew point temperature of the anode and cathode outlet gas streams which only depend

on the respective back pressures, stoichiometric flow ratios and the water balance [3]. A modeling study suggested that the resulting water balance may in fact be very close to the targeted value when these operating conditions are applied, and this was in good accord with previous experimental observations made by other groups [4, 5]. The benefit of operating PEMFC in such a way lies in the fact that no or very little liquid water leaves the cell; ideally all product water will leave the cell in the gas phase, which is important for the remaining system downstream of the fuel cell as well as for the fuel cell heat and water management. It was found that expanding the outgoing gases to atmospheric pressures directly behind the fuel cell leads to a decrease in the relative humidity from the targeted 100% at elevated pressure, and ideally the water will condense only after leaving the fuel cell system such as the fuel cell vehicle. This has also important implications for the thermal management as the latent heat of the product water would put an additional load on the coolant if it were to remain inside the fuel cell and for automotive fuel cells this would lead to larger required radiators for fuel cell vehicles. Hence, the focus of recent work of our group has been to operate fuel cell in such a way that both outlet gases are fully saturated without carrying liquid water out of the cell.

While the previously mentioned modeling study suggested that such *modus operandi* is in fact possible, it was also found that the membrane is partly dehydrated especially at the cathode outlet region/anode inlet region when the fuel cell operates in counter-flow mode. On the other hand, liquid water was predicted to occur in the center of the cell inside the porous media, and it was also observed that the local relative humidity exceeds 100% along the channel walls in the center of the cell which would give rise to channel condensation. These observations can conceivably be verified using e.g. neutron radiography for the prefixed operating conditions, but this is beyond the scheme of this work.

A logical next step is now to find ways of getting the membrane better hydrated under the same operating conditions. In an ensuing modeling study the role of the channel and land area width on the overall membrane hydration level was investigated, and the outcome was that the finest pitch of 0.5 mm – 0.5 mm yielded the highest membrane hydration and the lowest peak temperature [6]. The average membrane water content exceeded $\lambda = 10$ while a fully hydrated membrane has a hydration value of $\lambda \approx 14$ when equilibrated with water vapor [7], but in light of the fact that the incoming gases were completely dry this was initially considered satisfactory. In order to obtain even higher values, numerous material and geometrical parameters have to be studied. An earlier suggestion was to apply an MPL with micro-channels on the CL side to allow the liquid water to move from the wet regions to dry regions driven by the capillary pressure [8]. While it is clear that such micro-channels will lead to an increased electric contact resistance, it is generally assumed that the contact resistance between the CL and MPL is much smaller than between the GDL substrate and the bipolar plates. A further advantage of such channels may be to provide relieve to the liquid water that may become trapped under freezing conditions and allow for the water to easily expand [9].

It is the goal of this study to investigate conceptually the effect of such micro-channels on the liquid water distribution as well as the membrane hydration level for a given set of operating conditions.

MODEL DESCRIPTION

The fuel cell model used in this study has been extensively described in previous publications [10-12]. It is based on the formerly commercial software package CFX-4 (ANSYS Inc.), a classical *I, J, K*-structured, multi-block CFD code with leading capabilities in terms of multi-phase flow in conjunction with porous media. Salient features of our model are:

- Three-dimensional geometry that includes anode and cathode flow channels, bipolar plates, gas diffusion layers, micro-porous layers, catalyst layers and the polymer electrolyte membrane.
- Capability of modeling either conventional straight channel flow fields or interdigitated flow fields in co- or counter-flow mode.
- Multi-phase flow of water is described using the multi-fluid approach, i.e. one set of conservation equation is solved for each thermodynamic phase considered.
- Capillary action of liquid water through the porous media is described by the so-called Leverett function [13]. The fraction of hydrophilic pores inside porous media is accounted for by the irreducible saturation.
- Non-equilibrium phase-change of water is accounted for where the driving force is the deviation from full saturation. This accounts for the area of the liquid/gas interface.
- The model is non-isothermal. Thermal contact resistances between different solid layers (GDL and bipolar plates) are accounted for.
- The cathode side includes species equation for oxygen and water (liquid and gas) while the anode side includes hydrogen and water (liquid and gas).
- Three-dimensional model for water transport through polymer electrolyte membrane considering non-equilibrium absorption/desorption, electro-osmotic drag, diffusion and hydraulic permeation through the open pores.
- Simplified electro-chemistry that assumes a three-dimensional current density inside the CL's to calculate local sink and source terms of reactants inside catalyst layers; the pre-specified total current density corresponds to total amount of oxygen and hydrogen consumed and water and waste heat produced.

As is shown in Figure 2, the fact that an *I, J, K*-structured mesh is used allows for the computational disconnection of the different physical domains which is very convenient for modeling purposes.

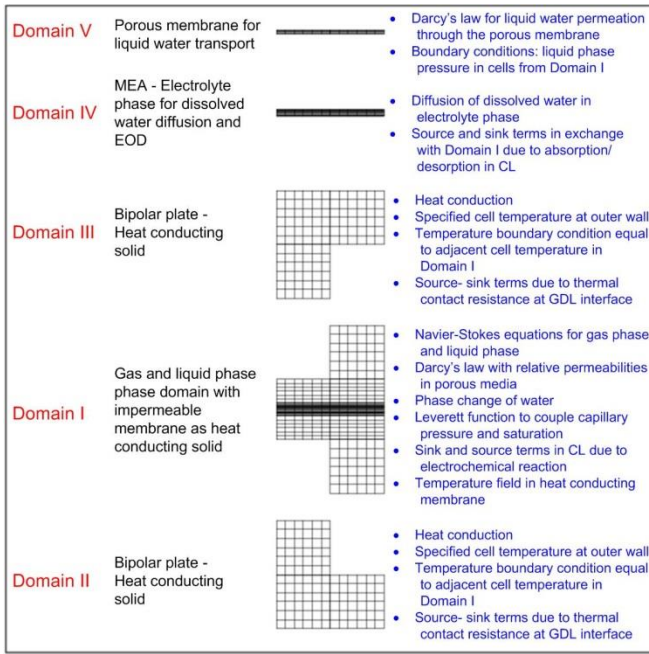


Figure 2 Computational domains and their modelling purposes with an exemplary numerical grid.

In general, *Domain I* is the main computational domain where the multi-phase flow and species equations are solved. *Domains II and III* represent the bipolar plates where currently we are only interested in the heat transfer equation. A temperature boundary condition is imposed at the outer surfaces where the coolant would be, and the cells bordering to the inner surfaces communicate with the corresponding neighboring cells of *Domain I*. *Domain IV* is a copy of the membrane and the CL's of *Domain I*. This sandwich is also called the membrane-electrode-assembly (MEA). However, in *Domain IV* we are only interested in calculating the transport of water that is dissolved in the electrolyte phase. Simply put, in order for the water to cross from cathode to anode in *Domain I*, it has to absorb from the cathode CL of *Domain I* to the corresponding control volume (CV) of *Domain IV*, diffuse through the electrolyte phase of *Domain IV*, and then desorb from the anode CL in *Domain IV* to the corresponding CV in *Domain I*. These absorption and desorption terms are accounted for as sink and source terms for the water transport equation in the respective domains. This appears complex, but it allows for a clean implementation of the water cross-over and is numerically very robust.

The salient feature of the study presented here is the addition of the effect of micro-channels in the computational model. Off-hand, it was clear that it was not possible to resolve these micro-channels with the numerical grid because this would have resulted in a prohibitive grid size given the complexity of the model, and it would have added undesired complexity to the physical model. In order to simplify the problem, it was decided to split the computational domain for the MPL into two regions: Region I included the micro-channels and region II was without micro-channels. These regions were assumed to be $30 \mu\text{m}$ thick. This means that

originally the MPL had an overall thickness of $60 \mu\text{m}$, and then micro-channels of a depth of $30 \mu\text{m}$ were carved into the MPL substrate. The width of these micro-channels is adjustable, depending on the carving tool. In the current study micro-channel widths of $30 \mu\text{m}$, $40 \mu\text{m}$ and $50 \mu\text{m}$ were investigated, respectively. The spacing of these channels was left constant at $100 \mu\text{m}$. Figure 3 shows schematically the set-up of a PEMFC including an MPL with micro-channels. The dimensions may be in the range of a few tens μm , and the MPL is essentially subdivided into two layers, one with a high permeability in the up and downstream direction (x -direction) and the second with an isotropic, lower permeability.

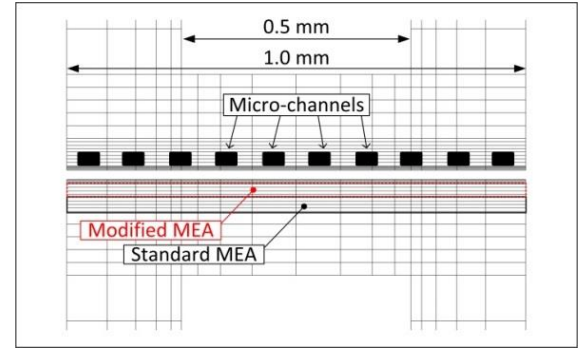


Figure 3 Schematic of the computational mesh and the location of the micro-channels. The upper part shows the location of micro-channels in the computational domain. In our model the micro-channels are accounted for by a smearing approach in a modified MPL domain, as indicated in the lower half.

In order to simulate the micro-channels in the three-dimensional computational fluid dynamics model the following reasoning was made: While we may assume Darcy type of flow in the porous media such as the CL's, MPL backing layer and gas diffusion layer (GDL), we may assume open channel flow in the micro-channels. Such flow is described by the Hagen-Poiseuille equation that generally relates the average channel velocity u to the pressure drop dp/dx according to the following equation:

$$u = -\frac{1}{32} \frac{D^2}{\mu} \frac{dp}{dx} \quad (4)$$

where D is the diameter of the pipe and μ is the hydraulic viscosity of the fluid, in this case water. This equation can be analytically derived by integrating the parabolic flow profile and using the definition of the hydraulic viscosity.

For a rectangular channel of height H and width W the hydraulic diameter D_H has to be used which is defined as:

$$D_H = 4 \times \frac{\text{Area}}{\text{Perimeter}} = 4 \times \frac{H \times W}{2(H+W)} = 2 \frac{H \times W}{H+W} \quad (5)$$

Hence, for a rectangular channel the Hagen-Poiseuille equation becomes:

$$u = -\frac{1}{8} \frac{(H \times W)^2}{(H+W)^2} \frac{1}{\mu} \frac{dp}{dx} \quad (6)$$

On the other hand, in our numerical model the three-dimensional convective flow through the various porous media is described by Darcy's law which reads for flow in the x -direction:

$$u = -\frac{K}{\mu} \frac{dp}{dx} \quad (7)$$

where K is the hydraulic permeability of the porous medium, given in [m^2]. Hence, it can be seen that in order to model the Hagen-Poiseuille equation using Darcy's law we need to replace the hydraulic permeability by the dimensions of the micro-channels:

$$K = \frac{1}{8} \frac{(H \times W)^2}{(H + W)^2} \quad (8)$$

Table 1 shows a comparison of chosen micro-channel dimensions and their corresponding hydraulic permeabilities according to equation (8).

Table 1 Micro-channel dimensions and their corresponding hydraulic permeability.

Channel dimensions, H×W [$\mu\text{m} \times \mu\text{m}$]	Hydraulic permeability, K [m^2]
30 × 30	28.1×10^{-12}
30 × 40	36.7×10^{-12}
30 × 50	44.0×10^{-12}

It is instructive to compare these values with experimental data of the hydraulic permeability for different types of gas diffusion layers which typically have pore sizes in the range of 10-30 μm . Depending on the direction, reported values for SGL type of paper range from 37-57 *Darcy* (1 *Darcy* = 10^{-12} m^2), while the denser Toray type has reported values ranging from 9-15 *Darcy* [14]. In this work the hydraulic permeability of the standard MPL is assumed to be one *Darcy*, hence it is more than one order of magnitude lower than the permeability in the channel direction of the micro-channels.

Now that a possibility was found to account for Hagen-Poiseuille flow with a Darcian model, additional adjustments had to be made to some other modeling parameters. Assuming that there will only be capillary action inside the micro-channels once they have been filled with liquid water over the entire cross-section of the channel, the irreducible saturation has to be set to $s_{irr} = 0.3, 0.4$ and 0.5 , respectively, in the modified MEA region. These values result out of the fact that the micro-channels have a pitch of 100 μm and a width of 30, 40 and 50 μm , respectively. Generally, the irreducible saturation in a porous medium accounts for the pore-fraction that is not subjected to capillary action.

Capillary pressure as a driving force only arises once the liquid saturation level exceeds the irreducible saturation, and the capillary pressure depends of the reducible saturation as described by the Leverett equation [13]:

$$p_{cap} = \sigma \cos \theta \left(\frac{\varepsilon}{K} \right)^{0.5} J(S) \quad (9)$$

Here, σ is the surface tension between the gas phase and the liquid phase, typically taken to be 0,625 N/m [15], θ is the contact angle of the liquid phase which depends on the surface treatment, e.g. amount of PTFE, ε is the porosity and K the permeability of the porous medium. The function $J(S)$ is usually a cubical function that describes the dependency of the capillary pressure on the reducible saturation S , defined as [16]:

$$S = \frac{s - s_{irr}}{1 - s_{irr}}, s \geq s_{irr} \quad (10)$$

Where s is the total liquid saturation and s_{irr} is the irreducible liquid saturation. Berning *et al.* [10] argued that the cubicle function $J(S)$ accounts for the pore-size distribution, a steeper function resulting from a wider PSD and leading to better liquid water transport compared to a flatter $J(S)$ function.

Now that the channel geometry and the area fraction of the channels in the MPL have been accounted for the question remains which capillary pressure function has to be applied for the liquid water transport inside the micro-channels. This can be answered out of the following consideration: Before the channel will be completely filled over the height and width, there is no liquid water pressure that could drive the water upstream or downstream. There will only be a capillary pressure inside the channels that can act as a driving force when the micro-channel is completely filled and the water starts to press into the adjacent MPL material. The capillary pressure curve of this material is given by the Leverett curve of the MPL material. Hence, the same capillary pressure function can be used to describe the channel flow as is used to describe the darcian flow through the MPL material.

To summarize: MPL with micro-channels have been accounted for by dividing the MPL into a region with and without the micro-channels. The region with micro-channels has a higher upstream and downstream permeability which is given out of the channel dimensions, it has a higher irreducible saturation to account for the fact that the channels first have to be filled with water over the entire cross-section before capillary actions starts pushing the water upstream and downstream, and the capillary pressure function that is needed to drive the water can be assumed identical to the function that describes the MPL substrate. The hydraulic permeability of the surrounding MPL material is more than one order of magnitude lower than the permeability of the region with micro-channels. More details as to how the capillary multi-phase transport in porous media can be implemented into CFX-4 can be found elsewhere [17, 18].

MODELING STUDY

The purpose of this study was to model the effect of micro-channels inside the MPL to guide the liquid water from wet regions towards the drier inlet and outlet regions. Such wet regions in the middle of the cell have been observed when the fuel cell operates in a way that both reactants (pure hydrogen and air) gases enter completely dry (0% relative humidity). The

detailed operating conditions such as anode and cathode pressure, stoichiometric flow ratios and inlet/outlet temperatures can be determined with the help of dew point diagrams so that both outlet gas streams may be exactly fully saturated to avoid liquid water leaving the cell. Table 2 summarizes the operating conditions used in this study. The low stoichiometric flow ratios necessitate the use of the interdigitated flow field which has better mass transport properties compared to the conventional parallel flow field. As was previously mentioned, when the water balance assumes an effective drag coefficient $r_d = -0.014$ both outlet streams will be exactly saturated with water vapour. The effective (or “net”) drag coefficient is defined as:

$$r_d = \frac{\dot{n}_{anodein}^{H_2O} - \dot{n}_{anodeout}^{H_2O}}{I/F} \quad (11)$$

Hence, it is the difference in the molar water stream between the anode inlet and the anode outlet which has been normalized by the total current I generated and Faraday’s constant F ($= 96485$ C/mole).

Table 2 Summary of operating conditions found with the help of dew point diagrams.

Property	Anode	Cathode
Inlet temperature [°C]	80	85
Stoichiometric flow ratio [-]	1.03	1.1
Inlet relative humidity [%]	0.0	0.0
Outlet pressure [atm]	1.2	1.5

As was mentioned above, the channel width and land area in the fuel cell was taken to be 0.5 mm each as this was found to yield the highest membrane hydration levels compared to wider pitches. The geometry was shown in Figure 3. In the current study, three different current densities were investigated, 0.4 A/cm², 0.8 A/cm² and 1.2 A/cm². For each of these current densities the case without micro-channels was investigated as well as the cases with micro-channels of 30, 40 and 50 microns width, respectively, yielding a total of 12 cases. The operating conditions and other material properties were left constant with the exception of the micro-channel region.

Sample Results

One of the salient features of our model compared to other publications is to automatically handle the interfaces between the various porous layers in terms of predicting the liquid water saturation jump. Because of the fact that the capillary pressure is a continuous function across the interface of two porous media with different Leverett functions, there will result a saturation jump across the interface between e.g. the CL and the MPL or the MPL and the GDL [16]. The advantage of employing the multi-fluid approach is that these saturation jumps are automatically predicted without adding computational cost. Figure 4 shows exemplarily the calculated liquid water saturation for the case with 50 μm wide micro-channels at a current density of 1.2 A/cm² in a layer near the cathode inlet/anode outlet section (“low x ”). The cell height is

the y -direction and the cell width the z -direction. The calculated results have been mirrored around the y -axis for better visualization. “Ca_I” denotes the inlet channel compartment of the cathode in the interdigitated design, and “Ca_II” the outlet compartment. The flow direction is thus from Ca_I through the porous media into Ca_II where the oxygen depleted air leaves the cell at the outlet located at *high-x*. The same is true for the anode, the only difference being that the anode inlet is at *high-x* and the hydrogen flows in the *low-x* direction. This can be seen in more detail in figures below. The flow arrangement is counter-flow, and this is necessitated by the fact that anode outlet and cathode outlet temperature are different and the anode outlet is the hot end of the cell, meaning that the coolant flow direction is co-flow to the anode gas stream (*high-x* to *low-x*).

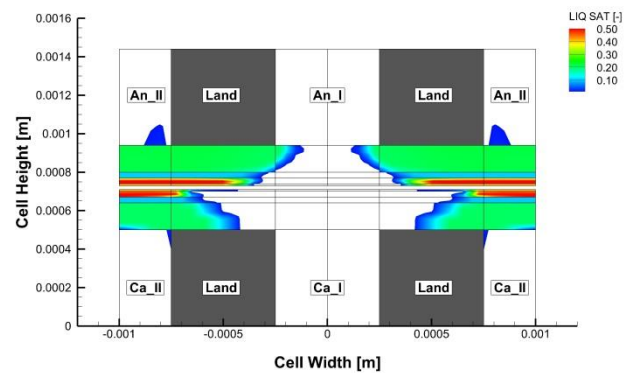


Figure 4 Calculated liquid saturation in an y - z -cut near the anode outlet/cathode inlet section (*low-x*). The anode side is the upper part and the cathode the lower part.

The liquid water distribution indicates that the anode side actually has a higher water content than the cathode side. The cut shown here is located near the anode outlet where the anode flow is fully humidified, and condensation in the hydrophilic regions is likely. The region where the liquid saturation exceeds 50% is the modified MPL region that contains the micro-channels. As the irreducible saturation is 50% here, the channels will have to be filled up entirely before capillary action drives the water upstream and downstream. It can be seen that the channels are filled only under land and beneath the outlet compartments (An_II and Ca_II). This has been observed throughout all cases investigated here, and this means that micro-channels only need to be carved in these regions and not underneath the inlet compartments (Ca_I and An_I). As the micro-channels lead to an increased contact resistance they should be applied only in regions where liquid water can be expected.

Between the modified MPL and the GDL substrate is the MPL backing without micro-channels. The same thickness of 30 microns was assumed, and the irreducible saturation was set to just 10% due to its high hydrophobicity. Moreover, the effective contact angle θ was assumed to be 150° , and this leads to the observed saturation jump between the MPL micro-channel regions and the MPL backing layer.

The next layer to the outside is the GDL substrate which also has different material properties. Here, the irreducible

saturation is assumed to be 20% and the effective contact angle θ is 120° . Again, the different material properties lead to the saturation jump between the MPL backing layer and the GDL. The “cut-off value” in Figure 4 is a liquid saturation of $s = 0.01$ and regions where the saturation is below this value are left blank. This shows that actually there is liquid water oozing from the GDL into the flow channels at both anode and cathode side. The resulting calculated water balance for this case was $r_d = -0.025$ which is below the target value of $r_d = -0.014$, and this means that the anode side is favored and there is some predicted (but undesired) liquid phase at the anode outlet.

A second result that shall be exemplarily shown is the calculated water transport between anode and cathode in the different regions of the cell. As was explained in detail in a previous publication [12], the conservation equation for the dissolved water inside the electrolyte phase reads:

$$-\frac{\rho^{mem}}{EW} \nabla \cdot (D_W^{mem} \nabla \lambda) M_W = \alpha \times k_a \times \frac{\rho^{mem}}{EW} (\lambda_{equil} - \lambda) \times M_W - \nabla \cdot \left(n_d \frac{I}{F} \right) M_W \quad (12)$$

Where λ denotes the water content of the electrolyte phase and λ_{equil} is the equilibrium value that depends on the relative humidity of the surrounding gas phase and has been measured by Zawodzinski *et al.* [7]. It is beyond the scope of this work to elaborate more on the terms in equation (12), and so the conservation equation of the water in the electrolyte phase shall simply be written as:

$$Diffusion = NES + EOD \quad (13)$$

Where the term on the left had side describes the diffusion of water that is dissolved in the electrolyte phase and the two terms on the right hand side are sink- or source terms for this water. NES denotes non-equilibrium sorption (or desorption) of water from/to the adjacent gas phase, and is dependent on the activity of the adjacent water in the gas or liquid phase. EOD is the electro-osmotic drag term that depends on the current density. The NES term is zero inside the membrane and non-zero inside the CL's, and if the EOD coefficient n_d is taken as a constant then this term also becomes zero in the membrane and it can be seen that the only water transport mechanism inside the membrane is in fact diffusion, as has been pointed out before [19].

Mathematically, the EOD term is a source term for electrolyte phase water in the anode CL, and a corresponding sink term in the cathode CL. Because of species conservation this water has to be taken from the anode gas phase and added to the cathode gas phase in the computational Domain I, respectively. Hence, the EOD term alone causes water to move from the anode gas phase into the cathode gas phase as has frequently been measured in experiments. The direction of the NES term depends on the operating conditions, but it usually counter-acts the EOD term. Importantly, the NES term can to a degree be controlled by adjusting the specific electrolyte surface area in the CL, termed α in equation (12). A high surface area can facilitate absorption at the cathode side, and

hence the water balance as described in equation (11) can become negative so that fuel cell can operate without external humidification.

Hence, the local water balance in a fuel cell is determined by the right hand side of equation (13). According to the sign convention adopted in this work, if the overall balance between NES and EOD is positive e.g. inside the cathode CL, this term becomes a source term at the cathode CL and a corresponding sink term at the anode CL, and water diffuses through the membrane from cathode to anode. Likewise, if the overall balance between NES and EOD is negative inside the cathode CL, this term is an overall sink term for the water in the cathode electrolyte phase, and a corresponding source term for the gas phase water here, while it is a sink term for the water in the electrolyte phase of the anode CK. Shortly put: Negative values in the cathode CL indicate water transport from anode to cathode and positive values indicate water transport from cathode to anode.

Figure 5 shows the calculated source- and sink terms in two different locations inside the cathode CL for the same case as Figure 4. The upper part is a layer very close to the membrane and the lower part in the middle of the CL. The overall thickness of the CL's in our model is 12 microns, and so the lower plane in Figure 5 is around 5 microns away from the membrane. The unit of these values is $[\text{kg}/\text{m}^3\text{-s}]$. It can be seen that water transport is strongly from anode to cathode in the first half from the cell (*low-x*) where the dry air enters, and it is from cathode to anode in the second half of the cell where dry hydrogen enters at the *high-x* interface in the An_I compartment. The strongly negative terms are also associated with a cooling term as the water evaporates from the membrane into the surrounding gas phase. However, there is a corresponding heating term at the anode CL where the water condenses into the membrane phase. Still, these cooling terms at the cathode CL may help to avoid too high peak temperatures as it is typically the cathode side where the highest overpotentials occur and thus the strongest heating terms are located.

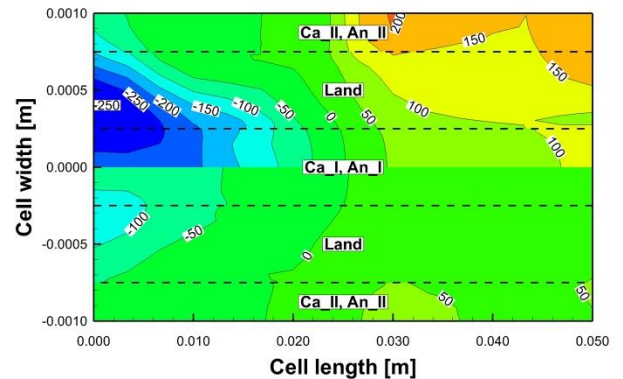


Figure 5 Sink and source terms for the electrolyte phase water inside the cathode CL close to the membrane (upper half) and in the middle of the CL (lower half). Negative values indicate water transport from anode to cathode and positive values from cathode to anode.

A comparison between the source and sink terms near the membrane and deeper into the CL shows that the terms near the membrane are substantially larger. This is probably good for the overall functionality of the water uptake layer that our group proposed in order to allow dry fuel cell operation [12]: while in this study the CL structure was assumed the same throughout the thickness, i.e. the specific surface area α was assumed constant over the CL thickness, the overall water balance is now found to be mostly determined very close to the membrane. It is not clear whether the roughness of the electrolyte phase inside the CL increases linearly with the CL thickness in practice, but apparently it does not seem to matter, and this is overall good news. The importance of the electrolyte phase roughness factor was highlighted in previous work [20].

Low current density cases

Detailed results shall be presented next for the low current density case of 0.4 A/cm^2 . It was previously pointed out that one intention to apply micro-channels was to divert liquid water upstream and downstream as well as to provide a pressure relieve at the interface between the CL and the MPL where delamination is sometimes observed under freezing conditions [9]. Figure 6 shows the calculated pressure distribution of the liquid water for the case without micro-channels and for the case with 30 microns wide micro-channels.

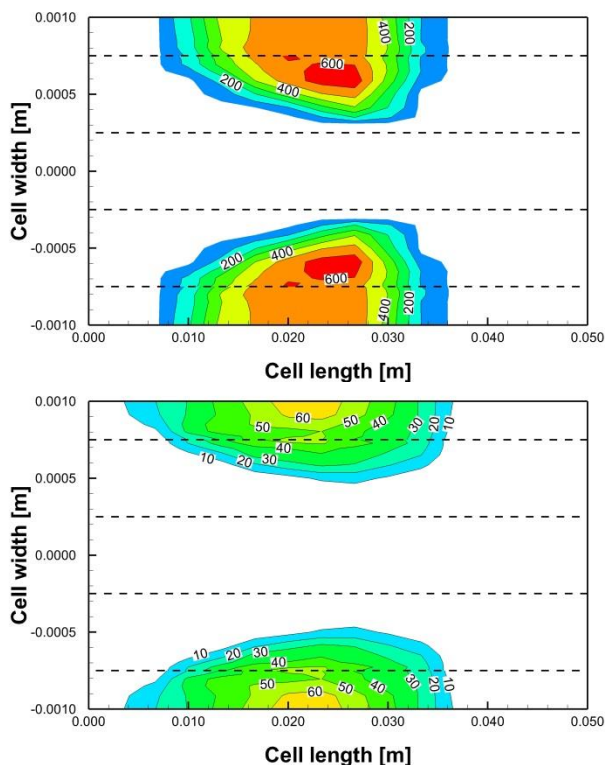


Figure 6 Calculated capillary pressure distribution [Pa] in an x - z -plane through the center of the micro-channel region for the case without micro-channels (upper) and with 30 microns wide micro-channels (lower).

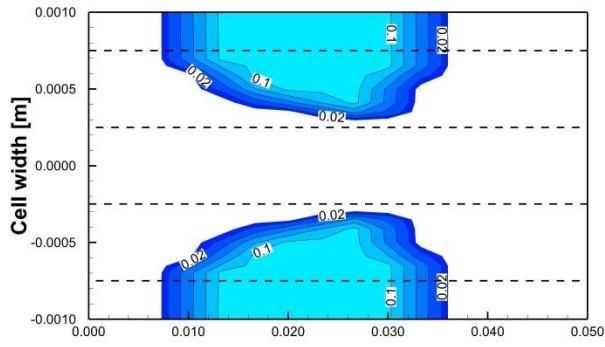
The plane is located in an x - z -cut through the modified MPL region where the micro-channels are located. The calculated capillary pressure in the case without micro-channels is substantially higher compared to the case with micro-channels, and hence the theory that the micro-channels provide pressure relieve seems to hold. It has to be understood that the detailed pressure distribution results out of the Leverett function used for the different porous layers and out the general operating conditions. In other cases capillary pressures exceeded 2000 Pa at the CL/MPL interface [10].

Figure 7 shows the liquid saturation distribution in the same x - z -plane through the micro-channel region. The liquid patch predicted inside the cell is roughly in the center of the cell, slightly towards the anode outlet ($low-x$). In the case without micro-channels the saturation is just around 10% and corresponds thus well with the irreducible saturation. As expected, when micro-channels are included the water spreads out towards the inlet and outlet region, and again the predicted saturation corresponds well with the applied irreducible saturation, and it can be clearly seen in which regions the channels are filled. It can be observed that underneath the entire inlet compartments Ca_I and An_I there is no liquid water predicted, and thus it makes no sense to include micro-channels here.

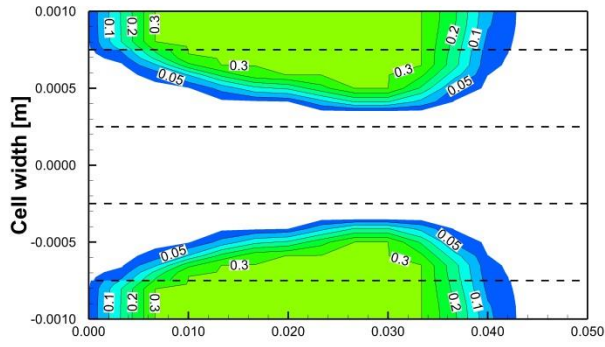
Figure 8 shows the resulting membrane water content for the low current density case. The regions of high membrane water content match quite well the regions where liquid water was predicted. The average water content increases slightly when micro-channels are included, as will also be summarized below. A problematic region appears to be the cathode outlet/anode inlet section ($high-x$) where the membrane water content decreases to values below $\lambda = 5$. This applies to the region between $x=0.04 \text{ m}$ and $x=0.05 \text{ m}$. Because the protonic conductivity of the membrane is a strong function of the membrane water content, membrane dehydration should be avoided. If this finding is verified experimentally, a simple remedy would be to just place the expensive platinum catalyst over the first 80% of the cell length and spare the dry membrane region. Thus, one may just use the membrane area that is sufficiently hydrated in order to generate current. While this would waste a small amount of the also expensive membrane, this part of the cell may be used as water exchange region. However, it must be admitted that this will of course also change the local current distribution and hence the local water formation rate. Our computational model can be adjusted to account for the fact that only a certain fraction of the cell is used to generate current, but it will require some complex modifications of our Fortran subroutines.

One reason for concern may be that, as is shown, the total cell length in this study is just 50 mm whereas real fuel cells have channel length of 200 mm and longer. However, it was previously found that the total channel length has only a small impact on the calculated results in our model.

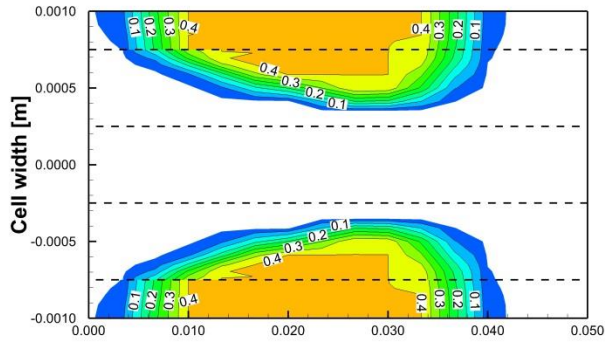
Overall it can be stated that the micro-channels area to fulfill their purpose to divert the water from the wet regions towards the drier inlet and outlet regions and thus yield a better hydrated membrane. A detailed comparison of the average membrane hydration levels will be given below.



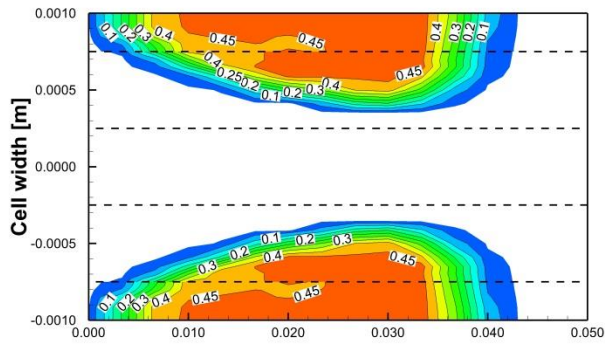
Cell length [m]



Cell length [m]

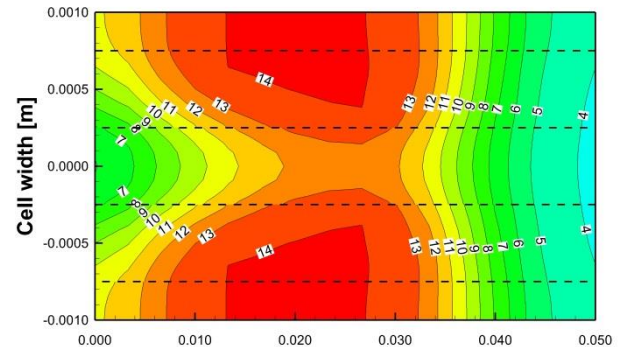


Cell length [m]

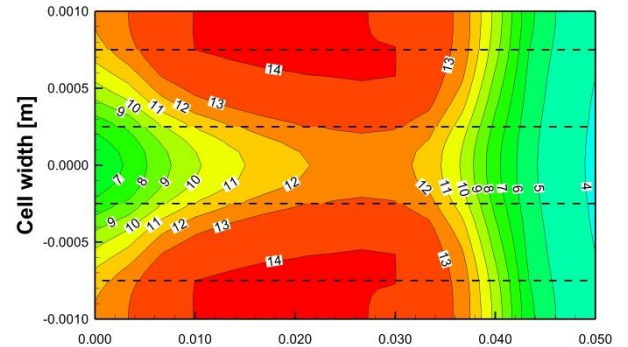


Cell length [m]

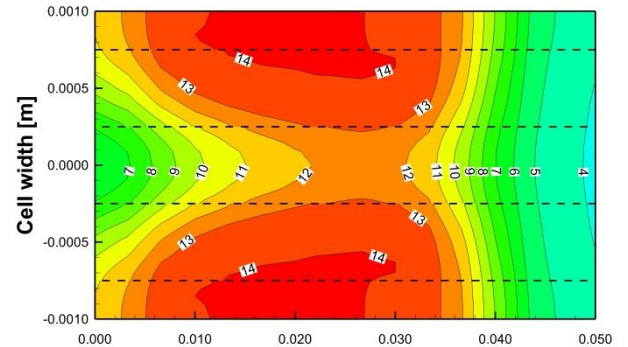
Figure 7 Liquid water saturation in the center of the cathode micro-channel region for the case without micro-channels (upper), and with micro-channels of 30 microns, 40 microns and 50 microns width (lower), respectively.



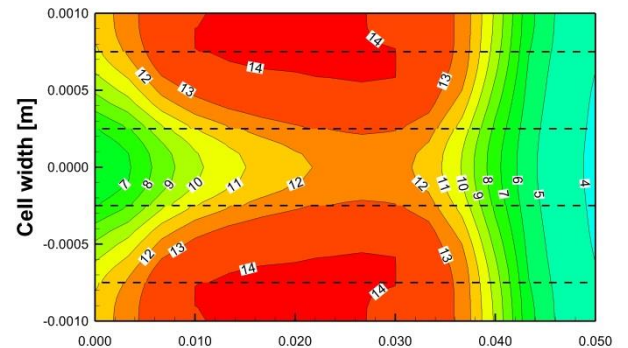
Cell length [m]



Cell length [m]



Cell length [m]



Cell length [m]

Figure 8 Water content λ in the center of the membrane for the case without micro-channels (upper), and with micro-channels of 30 microns, 40 microns and 50 microns width (lower), respectively.

Intermediate and high current density cases

For the sake of brevity only a few chosen results can be highlighted in this section. The first results discussed in detail include the calculated membrane hydration for the case of 50 microns wide micro-channels as these are consistently the cases with the highest membrane hydration levels. Figure 9 shows the membrane water content distribution for a current density of 0.8 A/cm^2 and 1.2 A/cm^2 . It is noted that the cathode outlet/anode inlet region becomes increasingly dry despite the fact that this is the cold end of the cell. Also, the average membrane hydration level decreases with increasing current density as will be shown below. This can be attributed to the increasing waste heat when the current density is increased. While frequently the argumentation is heard that at higher current density “more water” is being produced that helps to keep the membrane hydrated, this line of reasoning is flawed because the dew point temperatures which indicate the overall wetness of the cell are independent of the current density provided the stoichiometry is kept constant. However, a higher current density invariably leads to higher heating terms, and hence it leads to a drier membrane, not a wetter membrane, as long as the stoichiometric flow ratio is constant. The average value for the membrane hydration will be discussed below.

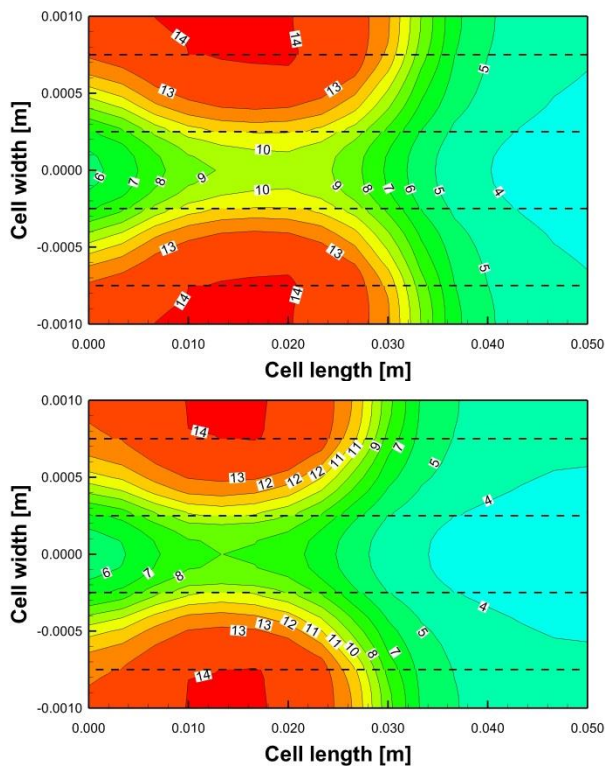


Figure 9 Water content λ in the center of the membrane for the case with micro-channels of $50 \mu\text{m}$ width for a current density of 0.8 A/cm^2 (upper) and 1.2 A/cm^2 (lower), respectively.

Figure 10 shows the calculated oxygen concentration inside the MPL close to the CL for the elevated current density cases. Once more the salient advantage of the interdigitated flow field is shown in that it has much better overall mass transport properties compared to the more popular straight channel flow

field that relies on diffusive oxygen transport to the CL. Given the fact that the stoichiometric flow ratio for oxygen/air was only $\xi = 1.1$ in these cases, the oxygen distribution is surprisingly uniform. Straight channel flow fields typically show a very strong non-uniformity with high oxygen concentration at the cathode inlet (*low-x*) under the channel and a much lower oxygen concentration at the cathode outlet (*high-x*) under land [21].

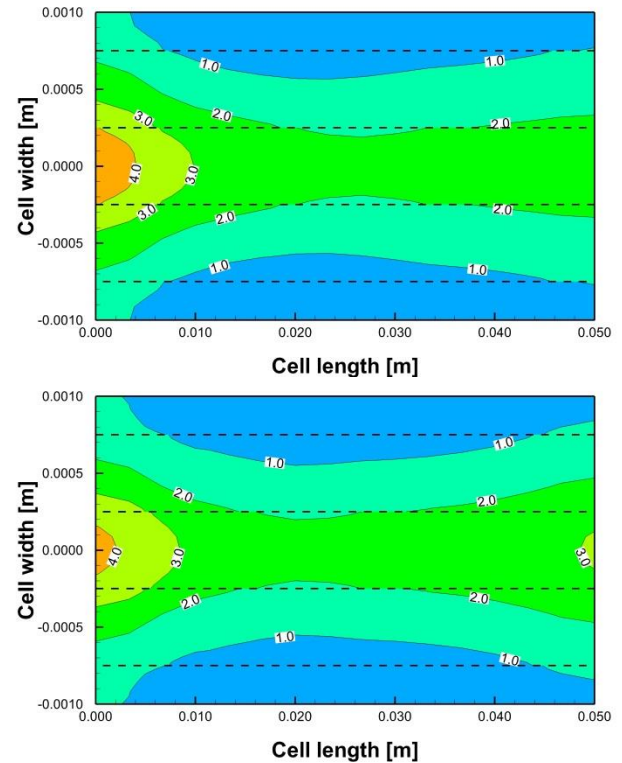


Figure 10 Oxygen concentration in the MPL close to the CL for the case with micro-channels of $50 \mu\text{m}$ width for a current density of 0.8 A/cm^2 (upper) and 1.2 A/cm^2 (lower), respectively.

Summary of results

Finally, the average membrane water content for all the cases shall be summarized. Figure 11 shows all cases investigated, and it can be seen that including micro-channels of 30 microns width leads to a notable increase in the membrane hydration level over having no micro-channels. Interestingly, the cases with 40 microns wide micro-channels showed nearly identical behaviour as the cases with 30 microns wide MC's, it is actually even slightly lower, while an increase in MC width to 50 microns yields another notable increase in the average membrane hydration. Hence, it would make sense to use micro-channels that are either 30 microns or 50 microns wide, while 40 microns width is not recommended because it increases the contact resistance but does not increase the membrane hydration level. However, such a statement is putting a lot of faith into these simulations. As usual, the final answer will have to come out of experiments, and these modelling simulations are meant to help understanding the underlying physics.

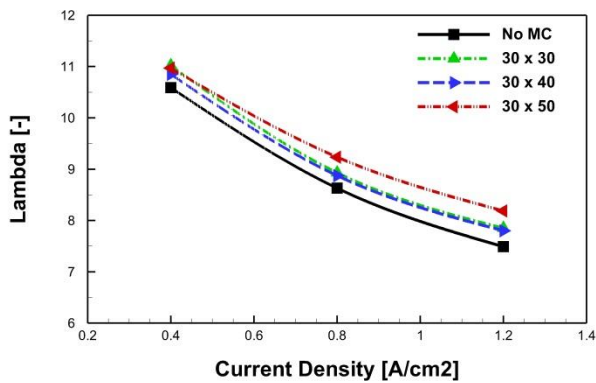


Figure 11 Average membrane hydration levels for all cases investigated.

CONCLUSION

Numerical simulations have been performed to investigate the effect of micro-channels in the micro-porous layer of a proton exchange membrane fuel cell on the expected membrane hydration level under pre-determined, optimized operating conditions. The micro-channels had a height of 30 microns while the width was assumed to be 30, 40, or 50 microns, respectively, and they were located at the interface between the catalyst layer and the MPL. The computational fuel cell model was adjusted so that the Hagen-Poiseuille equation was assumed in the micro-channels while the multiphase flow in the surrounding porous media was assumed to follow Darcy's law. It was found that micro-channels can provide a pressure relieve at the MPL/CL interface, and this might be important because it has been found by other groups that delamination of the fuel cell can occur at this interface under freezing conditions. Moreover, the liquid water patch that is typically encountered in the middle of the cell under such operating conditions is predicted to spread out and help to hydrate the membrane. The case of 30 micron wide channel resulted in a better hydrated membrane compared to having no micro-channels, and increasing the width to 50 microns gave another notable improvement, while 40 micron wide channels showed no improvement compared to 30 microns wide micro-channels. As the micro-channels will likely increase the contact resistance, using 40 microns wide channel makes no sense. Similar to previous simulations, the cathode outlet region experienced local membrane dehydration, despite this being the cold end of the cell. A proposed remedy was to not apply platinum catalyst in this region and hence not produce any current. Such effect could also be investigated with our computational model but it is left for future work.

ACKNOWLEDGEMENTS

This project has been sponsored by EUDP, J.nr. 64012-0117 and by PSO under the ForskEL program, Project nr.: 2013-1-12041.



REFERENCES

- [1] Berning, T., Three-dimensional computational analysis of transport phenomena in a PEM fuel cell, *PhD Dissertation*, University of Victoria (2002).
- [2] Berning, T., Employing dew point diagrams to optimize PEMFC operating conditions, *ECS Transactions* 50 (2012) 557-568.
- [3] Berning, T., The dew point temperature as a criterion for optimizing operating conditions of proton exchange membrane fuel cells, *J. Power Sources* 37 (2012) 10265-10275.
- [4] Büchi, F.N., Srinivasan, S., Operating Proton Exchange Membrane Fuel Cells Without External Humidification of the Reactant Gases, *J. Electrochem. Soc.* 144 (1997) 2767-2772.
- [5] Janssen, G.J.M., Overvelde, M.L.J., Water transport in the proton-exchange-membrane fuel cell: measurements of the effective drag coefficient, *J. Power Sources* 101 (2001) 117-125.
- [6] Berning, T., Multiphase Simulations and Design of Validation Experiments for Proton Exchange Membrane Fuel Cells, *ASME-FEDSM*, Incline Village, Nevada (2013).
- [7] Zawodzinski, T.A., et al., Water Uptake by and Transport Through Nafion 117 Membranes, *J. Electrochem. Soc.* 4 (1993) 1041-1047.
- [8] Berning, T., Fuel Cell Microporous Layer with Microchannels, *US Patent Application 0113,241*, (2007).
- [9] Kim, S., Mench, M.M., Physical degradation of membrane electrode assemblies undergoing freeze/thaw cycling: Micro-structure effects, *J. Power Sources* 174 (2007) 206-220.
- [10] Berning, T., Odgaard, M., Kær, S.K., A computational analysis of multi-phase flow through the porous media of a PEMFC cathode using the multi-fluid approach, *J. Electrochem. Soc.* 156 (2009) B1301.
- [11] Berning, T., Odgaard, M., Kær, S.K., A study of multi-phase flow through the cathode side of an interdigitated flow field using a multi-fluid model, *J. Power Sources* 195 (2010) 4842-4852.
- [12] Berning, T., Odgaard, M., Kær, S.K., Water balance simulations of a polymer-electrolyte membrane fuel cell using a two-fluid model, *J. Power Sources* 196 (2011) 6305-6317.
- [13] Leverett, M.C., Capillary behavior in porous solids, *Trans. AIME* 142 (1976) 152.
- [14] Gostick, J.T., Ioannidis, M.A., Fowler, M.W., Pritzker, M.D., Pore network modeling of fibrous gas diffusion layers for polymer electrolyte membrane fuel cells, *J. Power Sources* 173 (2007) 277-290.
- [15] Wang, Z.H., Wang, C.Y., Chen, K.S., Two-phase flow and transport in the air cathode of proton exchange membrane fuel cells, *J. Power Sources* 94 (2001) 40-50.
- [16] Nam, J.H., Kaviani, M., Effective diffusivity and water-saturation distribution in single- and two-layer PEMFC diffusion medium, *Int. J. Heat and Mass Transfer.* 46 (2003) 4595-4611.
- [17] Berning, T., Djilali, N., A 3D, multiphase, multicomponent model of the cathode and anode of a PEM fuel cell, *J. Electrochem. Soc.* 150 (2003) A1589-A1598.
- [18] Gurau, V., Zawodzinski, T.A., Mann, J.A., Two-phase transport in PEM fuel cell cathodes, *J. Fuel Cell Science and Technology* 5 (2008) 021009.
- [19] Berning, T., On water transport in polymer electrolyte membranes during the passage of current, *Int. J. Hydrogen Energy* 36 (2011) 9341-9344.
- [20] Berning, T., Kær, S.K., Low stoichiometry operation of a proton-exchange membrane fuel cell employing the interdigitated fuel cell – a modeling study, *Int. J. of Hydrogen Energy* 37 (2012) 8477-8489.
- [21] Berning, T., Lu, D.M., Djilali, N., Three-dimensional computational analysis of transport phenomena in a PEM fuel cell, *J. Power Sources* 106 (2002) 284-294.